Optical absorption and fluorescence intensities of Nd^{3+} in the garnets $CaY_2Mg_2Ge_3O_{12}$ and $Gd_3Ga_5O_{12}$ and the biaxial crystal $La_2Be_2O_5$

T. S. Lomheim* and L. G. De Shazer†
Departments of Physics and Electrical Engineering, University of Southern California, Los Angeles, California 90007
(Received 1 December 1978)

The Judd-Ofelt (JO) theory was applied to interpret the optical-absorption intensities of trivalent neodymium (Nd^{3+}) in the garnets $CaY_2Mg_2Ge_3O_{12}$ and $Gd_3Ga_5O_{12}$ and the biaxial crystal $La_2Be_2O_5$ yielding the JO parameters Ω_2, Ω_4, and Ω_6. The JO theory applied to the $^4F_{3/2}$ fluorescence transition in Nd^{3+} predicts a linear relation between the ratio R of the 1.06- to 1.35-μm fluorescence band intensities and the ratio Ω_4/Ω_6 of JO intensity parameters. This linearity was verified by independent measurements of R and Ω_4/Ω_6 for a series of Nd^{3+}-doped crystals and was found to be dependent on the type of free-ion wave functions that were used in calculating the required transition-matrix elements.

I. INTRODUCTION

Electric-dipole transitions responsible for the sharp-line optical spectra of rare-earth (RE) ions in crystals occur within the $4f$ configuration. Electric-dipole transitions are parity forbidden (Laporte rule[1]) if the electron responsible for the transition is in a force field which has a center of symmetry. As Van Vleck[2] first pointed out, the presence of the crystal spectra could be due to forced electric-dipole transitions, magnetic-dipole transitions, or electric-quadrupole transitions. The first of these mechanisms is the dominant one in the case of crystal spectra. A forced electric-dipole transition occurs when the electric field in which the optical electrons move lacks inversion symmetry. This occurs when a RE atom is placed in a crystalline environment which lacks inversion symmetry. Parity (the eigenvalue of the inversion operator) is no longer a good quantum number. The odd components of the crystal-field potential mix opposite parity configurations (such as $4f^{n-1}5d$, $4f^{n-1}5g$) into the $4f^n$ configuration. Thus a strictly parity-forbidden transition for the free ion becomes weakly allowed in the presence of the crystal field. A quantitative theory describing parity-forbidden transitions in rare earths was introduced simultaneously and independently by Judd[3] and Ofelt[4] known as the Judd-Ofelt (JO) theory.

In the JO theory the transition probability between any two J manifolds $|J\rangle$ and $|J'\rangle$ within the ground $4f^n$ configuration of a trivalent rare earth can be written in terms of three phenomenological intensity parameters denoted by Ω_2, Ω_4, and Ω_6. These parameters are determined experimentally by fitting the theoretical line strengths to corresponding line strengths, measured in absorption. The JO intensity parameters can then be used to calculate the transition probability between any pair of J manifolds, including fluorescence or excited-state absorption transitions which are inaccessible to direct measurement by absorption techniques. The JO parameters Ω_2, Ω_4, and Ω_6 have been measured for a large number of RE laser materials.[5–12] The most prominent rare earth in laser applications is trivalent neodymium (Nd^{3+}) which yields wavelengths of 0.9, 1.06, and 1.35 μm when doped in a variety of different hosts.

In this investigation the optical-absorption intensities of Nd^{3+} in $Y_3Al_5O_{12}$, $Gd_3Ga_5O_{12}$, $CaY_2Mg_2Ge_3O_{12}$, $La_2Be_2O_5$, and YVO_4 were measured. The results for $Y_3Al_5O_{12}$:Nd^{3+} are not listed here since our measurements agree to within 5% with previous work.[5] In the particular case of YVO_4:Nd^{3+} where the host material is a uniaxial crystal, special consideration to the directional effects of the absorption intensities had to be made in applying the JO theory with the specific details and results being reported in a separate publication.[13] The experimental data and JO fits to Nd^{3+} in $Gd_3Ga_5O_{12}$, $CaY_2Mg_2Ge_3O_{12}$, and $La_2Be_2O_5$ are found in Sec. IV of this paper.

The JO theory applied to the $^4F_{3/2}$ fluorescence transition in Nd^{3+} predicts a linear relation between the ratio R of the 1.06- to 1.35-μm fluorescence band intensities and the ratio Ω_4/Ω_6 of JO intensity parameters. In order to verify this linearity experimentally the fluorescence spectra of several Nd^{3+}-doped crystals and glasses were measured from 1.0 to 1.45 μm corresponding to the $^4F_{3/2}\rightarrow{}^4I_{11/2}$ (1.06 μm) and $^4F_{3/2}\rightarrow{}^4I_{13/2}$ (1.35 μm) transitions. For a particular Nd^{3+}-doped crystal the parameter R was obtained by this measurement and the corresponding Ω_4/Ω_6 factor was obtained by a JO fit of the absorption-band strengths. The predicted linearity was found to be dependent on the type of free-ion wave functions that were used in calculating the matrix elements required in the JO line-strength equation.

II. EXPERIMENTAL

A. Absorption and refractive-index measurements

A Cary 17 spectrophotometer was used to measure the absorption spectrum at room temperature from 0.3 to 1.8 μm for the Nd^{3+}-doped crystals. The spectrophotometer was operated in the absorbance mode and the integrated absorbances were measured with a planimeter. When two or more absorption manifolds were overlapped, the total integrated absorbance of the manifolds was treated as a single experimental point.

The theoretical fitting procedure used in this study, which is described in Sec. III, requires knowledge of the dispersion of the refractive indices over the wavelength range of the absorption spectrum. Since no published values of refractive indices of $CaY_2Mg_2Ge_3O_{12}$ were available they were measured by the method of minimum deviation. The prism used had faces 4.5 $\times$ 6 mm with prism angle of 42° 30′ measured to an accuracy of 30 sec of arc. A Spencer spectrometer (American Optical Company) was used to make angular measurements, and a helium-neon laser, argon-ion laser, mercury lamp, and hydrogen lamp were used as light sources for 11 wavelengths from 4341 to 6563 Å. The experimental data were least-squares fit to the Sellmeier equation

$$n^2 = 1 + A\lambda^2/(\lambda^2 - B) \quad . \tag{1}$$

The Sellmeier coefficients determined by least-squares fit are $A = 2.2888$ and $B = 0.01455$ μm^2 for $CaY_2Mg_2Ge_3O_{12}$. The measured and calculated refractive indices are tabulated in Table I, with the accuracy of the indices being ± 0.0005.

TABLE I. Measured and calculated indices of refraction of $CaY_2Mg_2Ge_3O_{12}$ at 300 °K.

λ (Å)	n_{meas}	n_{calc}
4341	1.8659	1.8656
4358	1.8654	1.8651
4861	1.8543	1.8545
4880	1.8536	1.8541
4916	1.8531	1.8535
5145	1.8498	1.8499
5461	1.8460	1.8459
5771	1.8424	1.8421
5790	1.8424	1.8421
6328	1.8372	1.8371
6563	1.8354	1.8355

Sellmeier Coefficients
$A = 2.2888$
$B = 0.01455$ μm^2

B. Fluorescence measurements

The fluorescence intensity measurements for the Nd^{3+}-doped samples were made using an optical assembly with a 0.5-m spectrometer (Jarrell-Ash) with an argon-ion laser (Coherent Radiation Model 52) used to excite the fluorescence. Detection was accomplished by means of an uncooled PbS detector and a lock-in amplifier (Princeton Applied Research Model 124).

The anisotropic samples that were studied possessed strongly polarized fluorescence spectra with π and σ polarizations exhibiting different radiation angular distribution patterns. Since the spectrometer grating sensitivity depended strongly on polarization, it was necessary to spatially average and depolarize the fluorescence spectra. This was accomplished by constructing an integrating sphere out of MgO which acted as a diffuse reflector with approximately 93% reflectivity. The integrating sphere was constructed actually in the shape of a box with two openings, one to allow entrance of the pump radiation, and the other for exiting fluorescence. A sample was placed inside this box in such a way that no direct fluorescence could be viewed by the spectrometer. The diffuse reflections of the fluorescence angularly integrated each component as well as depolarizing them.

The relative spectral response of the detection system was determined by using a standard blackbody lamp calibrated at the National Bureau of Standards. The fluorescence scan of each of the bands (1.06 and 1.35 μm) was point by point corrected for the relative spectral response and point by point multiplied by λ. The areas under these curves, which represented the fluorescence intensities on a photon basis were measured using a compensating polar planimeter (K&E 620015). The ratio of the 1.06 to 1.35 μm intensities R was a key experimental parameter.

III. THEORY

A. Judd-Ofelt theory

In free RE ions the matrix elements of the dipole operator vanish between eigenstates of the same parity. Hence, for a trivalent RE ion in a crystalline environment it was necessary to mix into the $4f^n$ configuration other configurations of opposite parity. Such mixing is caused by the odd components of the crystal-field potential which are present for crystals lacking inversion symmetry. For RE ions in crystals, the JO theory accounts for the presence of parity-forbidden electric-dipole transitions by the odd part

of the electrostatic crystal-field potential. The line strength for a transition between an initial J manifold $|4f^nJM_J\rangle$ and final manifold $|4f^nJ'M_{J'}\rangle$ is

$$S(J,J') = \sum_{\lambda=2,4,6} \Omega_\lambda |\langle 4f^nJM_J || U^{(\lambda)} || 4f^nJ'M_{J'}\rangle|^2 . \quad (2)$$

The $\Omega_{\lambda=2,4,6}$ are three phenomenological parameters that contain parameters from the crystal-field potential, interconfigurational radial integrals, and energy demoninators obtained from the perturbation expansion of the wave function. The matrix elements $|\langle || U^{(\lambda)} || \rangle|$ are doubly reduced unit-tensor operators calculated in the intermediate-coupling approximation,[14] since the electrostatic and spin-orbit energies are of comparable strength for RE ions. In the free-ion case the wave functions are linear combinations of LS or Russell-Saunders states

$$|4f^nJM_J\rangle \equiv |4^n[S,L],J\rangle = \sum_{S,L} C(S,L,J)|S,L,J\rangle \quad , \quad (3)$$

where $C(S,L,J)$ are the intermediate-coupling coefficients. In the notation of Eq. (3), the spin and angular-momentum quantum numbers (S,L) are not good quantum numbers but rather are convenient labels for the intermediate coupled states. The intermediate coupling coefficients $C(S,L,J)$ used in this study were obtained by Crosswhite,[15] and the corresponding matrix elements are listed in Ref. 13.

The integrated absorbance Γ of an electric-dipole transition within the $4f^n$ ground configuration of a rare-earth ion is given by

$$\Gamma = \int_0^\infty \alpha(\lambda)\, d\lambda = \frac{1}{L}\int_0^\infty \ln\frac{I_0}{I(\lambda)}\, d\lambda \quad , \quad (4)$$

where L is sample length, I_0 is the incident intensity, and $I(\lambda)$ is the transmitted intensity. The integrated absorbance Γ is related to the line strength by

$$\Gamma = \frac{4\pi^2 N\alpha_f \bar{\lambda}(n^2+2)^2}{3(2J+1)9n} S(J,J') \quad , \quad (5)$$

where N is the RE-ion concentration, α_f is the fine-structure constant, $\bar{\lambda}$ is the mean transition wavelength, n is the refractive index of the host material at $\bar{\lambda}$, and J is the total-angular-momentum quantum number of the initial manifold. Similarly the total spontaneous emission probability $A(J,J')$ for an electric-dipole transition between an excited state $|4f^nJ,M_J\rangle$ and a lower state $|4f^nJ',M_{J'}\rangle$ is

$$A(J,J') = \frac{32\pi^3\alpha_f c}{3(2J+1)} \frac{n(n^2+2)^2}{9\bar{\lambda}^3} S(J,J') \quad , \quad (6)$$

where c is the speed of light. Using Eq. (6) the total radiative lifetime of the excited manifold is

$$\frac{1}{\tau_{\text{rad}}} = \sum_{J'} A(J,J') \quad , \quad (7)$$

where the sum is over all final lower lying states, J', and the intermanifold branching ratio between states $|4f^nJ,M_J\rangle$ and $|4f^nJ',M_{J'}\rangle$ is

$$\beta(J,J') = \frac{A(J,J')}{\sum_{J} A(J,J')} \quad , \quad (8)$$

where J and J' label the initial and terminal manifolds, respectively, and the sum is over all the terminal manifolds J'.

B. Fitting calculation

The intensity parameters Ω_2, Ω_4, and Ω_6 are obtained by a least-squares-fitting procedure. First the experimental line strength $S_i^{(e)}$ is determined by the expression

$$S_i^{(e)} = \Gamma_i \left[\frac{3(2J+1)9n}{4\pi^2 N\alpha_f \bar{\lambda}(n^2+2)^2}\right] \quad , \quad (9)$$

which is Eq. (5) rewritten. Γ_i is the integrated absorbance of the ith absorption band of the ion in the crystal. The ion density N must be measured as well as the refractive index n. The measured absorption bands usually range from 0.3 to 1.5 μm, therefore the refractive index of the host material must be known over this wavelength region. The factor $(n^2+2)^2/9n$ which appears in Eqs. (5) and (6) is the local-field correction at the dipole due to the dielectric.[16] For refractive indices near 2 (which is the case for most of the crystals examined in this study) it can be seen that slight variations in index can lead to substantial variation in this factor. Hence it is important to know the refractive indices of the different absorption band wavelengths accurately. This is accomplished by measuring the refractive indices of the host material at specific wavelengths and then fitting the resulting data by least squares to the Sellmeier equation. Once the Sellmeier coefficients are determined the refractive index can be computed at any wavelength.

With the value of $S_i^{(e)}$ determined by Eq. (9) we then write out the theoretical expression for the line strengths $S_i^{(t)}$ given by the JO Eq. (2). The equation for calculating the reduced matrix elements that appear in $S_i^{(t)}$ is given in Sec. IV B of this paper. The theoretical line strengths can be expressed as

$$S_i^{(t)} = \sum_{j=1}^{3} U_i^{(2j)} \Omega_{2j} \quad , \quad (10)$$

where $i = 1, 2, \ldots, N$, and N is the number of absorption bands fitted. In the least-squares-fitting procedure we wish to minimize the quantity

$$\Delta = \sum_{i=1}^{N} (S_i^{(e)} - S_i^{(t)})^2 \quad , \quad (11)$$

with respect to the parameters Ω_2, Ω_4, and Ω_6. This is accomplished by differentiating Δ with respect to the Ω_λ parameters. In other words

$$\frac{\partial}{\partial \Omega_{2l}} \sum_{i=1}^{N} \left[S_i^{(e)} - \sum_{j=1}^{3} U_i^{(2j)} \Omega_{2j} \right] = 0 \ , \qquad (12)$$

with $l = 1, 2, 3$. This leads to three equations in three unknowns which are then solved for Ω_2, Ω_4, and Ω_6.

IV. RESULTS AND ANALYSIS

A. JO fit to Nd^{3+} in cubic $Gd_3Ga_5O_{12}$ and $CaY_2Mg_2Ge_3O_{12}$ and biaxial $La_2Be_2O_5$

The measurable absorption bands of Nd^{3+} extend from 3000 to 24 000 Å in most crystal and glass hosts. Measurements of the uv bands is usually limited by color center absorption that masks some of the weaker bands. In our study we perform absorbance measurements from the uv absorption edge out to 18 000 Å for Nd^{3+} in $Gd_3Ga_5O_{12}$, $Y_3Al_5O_{12}$, $CaY_2Mg_2Ge_3O_{12}$, $La_2Be_2O_5$, and YVO_4.

Since the JO Eq. (2) has no polarization or angular details the total integrated absorbances (over direction and polarization) are required in a fit to the theory. For optically isotropic materials (cubic crystals and glasses) this presents no difficulty. The crystals $CaY_2Mg_2Ge_3O_{12}$:Nd^{3+} and $Gd_3Ga_5O_{12}$:Nd^{3+} are cubic and therefore the absorption spectrum can be measured along any direction of the sample. For the case of biaxial crystals such as $La_2Be_2O_5$:Nd^{3+} the absorption spectrum is very complex and somewhat different in structure when measured along the three crystallographic directions. The absorption strengths band for band, however, stay about the same (within 5%) when measured along these three crystallographic directions. The complicated optical anisotropy properties of biaxial crystals tend to depolarize and directionally average the spectra. Figure 1 shows a comparison of three absorption bands (centered at 4300, 4700, and 6900 Å) measured along the three crystallographic directions X, Y, Z of a 1-cm cube of $La_2Be_2O_5$:Nd^{3+}. (The strength of these absorption bands vary no more than 5% along the three crystallographic directions X, Y, Z.) Therefore as in the case of cubic crystals the absorption spectrum may be measured along any crystallographic direction and applied to the JO theory without much error. The best procedure is to simply average the absorption strengths of each band over the three directions.

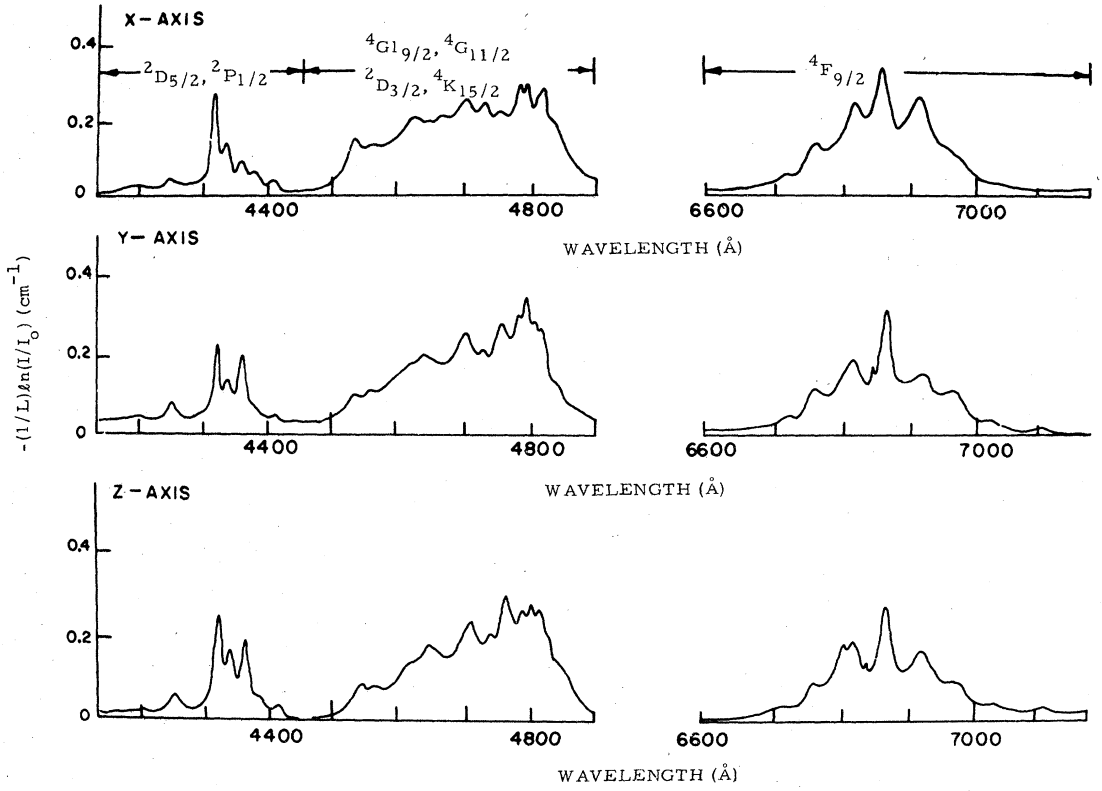

FIG. 1. Absorption spectrum along the X, Y, Z crystallographic axes of a 1-cm cube of $La_2Be_2O_5$:Nd^{3+}. L is the sample length.

For a uniaxial crystal such as $YVO_4:Nd^{3+}$ this averaging procedure cannot be blindly applied. Certain conditions must be met if the procedure is to give meaningful results. For this reason the JO fit to $YVO_4:Nd^{3+}$ is treated as a special case in a separate publication.[13]

Literatures values for refractive indices were available for all of the crystals except $CaY_2Mg_2Ge_3O_{12}$ which were measured and are listed in Table I. The resulting Sellmeier equation is

$$n^2 = 1 + 2.2888\,\lambda^2/(\lambda^2 - 0.01455)\ , \tag{13}$$

where λ is measured in μm. For $Gd_3Ga_5O_{12}$ and $Y_3Al_5O_{12}$ we use the Sellmeier equations from Ref. 17. They are

$$n^2 = 1 + 2.7382\,\lambda^2/(\lambda^2 - 0.01755)\ , \tag{14}$$

$$n^2 = 1 + 2.2779\,\lambda^2/(\lambda^2 - 0.01142)\ , \tag{15}$$

respectively.

For $La_2Be_2O_5$, n vs λ were taken from Jenssen *et al.*[18] who report refractive indices n_x, n_y, and n_z (x, y, and z correspond to the three crystallographic directions) from 0.6 to 2.0 μm. These data were fit to three Sellmeier equations resulting in

$$n_x^2 = 1 + 2.7990\,\lambda^2/(\lambda^2 - 0.01875)\ , \tag{16}$$

$$n_y^2 = 1 + 2.9268\,\lambda^2/(\lambda^2 - 0.01918)\ , \tag{17}$$

$$n_z^2 = 1 + 3.0725\,\lambda^2/(\lambda^2 - 0.01950)\ . \tag{18}$$

With these Sellmeier equations the factor $\chi = (n^2+2)^2/9n$ (local-field correction at the dipole due to the dielectric) was computed for each absorption band of Nd^{3+} in the various hosts.

In the particular case of $La_2Be_2O_5:Nd^{3+}$ an effective χ was calculated which was the average of χ_x, χ_y, χ_z calculated with the corresponding indices n_x, n_y, n_z. As mentioned before, the weak absorption bands shown in Fig. 1 have the same strengths with 5% along the three directions. Stronger bands, however, were not measured since the ion density and path length of the $La_2Be_2O_5$ cube were such that the absorbances were too high for meaningful measurement. A wafer of $La_2Be_2O_5:Nd^{3+}$ of 0.108 cm length, oriented along the X axis, was used for the stronger absorbances. For stronger absorbances it is expected that the differences with crystallographic direction would be small as in the case of the weak bands.

The integrated absorbances were measured with a compensating polar planimeter (K&E 620015) after Fresnel reflection losses were subtracted from the absorption curves. When two or more absorption manifolds were overlapped, the total integrated absorbance of the manifolds was treated as a single experimental point. The integrated absorbances were converted to line strengths by Eq. (9) and then used in the JO fit given by Eq. (12). The required reduced matrix elements were taken from Table I of Ref. 13. Tables II, III, and IV tabulate the integrated absorbances and corresponding measured and calculated line strengths for Nd^{3+} in $Gd_3Ga_5O_{12}$,

TABLE II. Absorbances, measured S_m, and calculated S_c line strengths for $Gd_3Ga_5O_{12}:Nd^{3+}$[b] at 300 °K.

Excited state $\lvert 4f^n[S',L'],J'\rangle$	λ (Å)	$\int \alpha(\lambda)\,d\lambda \left(\frac{\text{Å}}{\text{cm}}\right)$	S_m[a]	S_c[a]	$(\Delta S)^2$
$^4I_{13/2}$	24 000	. . .	. . .	1.709	. . .
$^4I_{15/2}$	16 000	47.60	0.299	0.166	0.0178
$^4F_{3/2}$	8 800	67.13	0.759	0.947	0.0351
$^4F_{5/2}, {}^2H2_{9/2}$	8 050	237.29	2.927	2.687	0.0574
$^4F_{7/2}, {}^4S_{3/2}$	7 450	194.63	2.586	2.563	0.0005
$^4F_{9/2}$	6 800	17.12	0.248	0.177	0.0051
$^2H2_{11/2}$	6 250	4.88	0.076	0.047	0.0008
$^4G_{5/2}, {}^2G1_{7/2}$	5 850	131.70	2.201	2.222	0.0004
$^4G_{7/2}, {}^4G_{9/2}, {}^2K_{13/2}$	5 250	78.60	1.452	1.185	0.0715
$^2G1_{9/2}, {}^2D_{3/2}, {}^2K_{15/2}$	4 700	23.19	0.474	0.287	0.0349
$^2D_{5/2}, {}^2P_{1/2}$	4 350	4.76	0.104	0.141	0.0013
$^4D_{3/2}, {}^4D_{5/2}, {}^2I_{11/2}$ $^4D_{1/2}, {}^2L_{15/2}, {}^2I_{13/2}$ $^4D_{7/2}, {}^2L_{17/2}$	3 500	74.09	1.941	2.060	0.0142

[a]In units of 10^{-20} cm^2.

[b]Sample length 0.491 cm.

TABLE III. Absorbances, measured S_m, and calculated S_c line strengths for $CaY_2Mg_2Ge_3O_{12}:Nd^{3+}$[b] at 300 °K.

Excited state $\|4f^n[S',L'],J'\rangle$	λ (Å)	$\int\alpha(\lambda)d\lambda\left[\frac{\text{Å}}{\text{cm}}\right]$	S_m^a	S_c^a	$(\Delta S)^2$
$^4I_{13/2}$	24 000	...	...	...	...
$^4I_{15/2}$	16 000	137.13	0.270	0.200	0.0050
$^4F_{3/2}$	8 800	215.79	0.768	0.917	0.0221
$^4F_{5/2}, {}^2H2_{9/2}$	8 050	845.07	3.285	3.010	0.0761
$^4F_{7/2}, {}^4S_{3/2}$	7 450	662.91	2.781	3.047	0.0710
$^4F_{9/2}$	6 800	53.10	0.244	0.205	0.0015
$^2H2_{11/2}$	6 250	11.86	0.059	0.055	...
$^4G_{5/2}, {}^2G1_{7/2}$	5 840	547.37	2.912	2.937	0.0006
$^4G_{7/2}, {}^4G_{9/2}, {}^2K_{13/2}$	5 240	270.86	1.599	1.269	0.1092
$^2G1_{9/2}, {}^2D_{3/2}, {}^2K_{15/2}, {}^4G_{11/2}$	4 680	78.80	0.514	0.300	0.0455
$^2D_{5/2}, {}^2P_{1/2}$	4 320	13.83	0.097	0.129	0.0010
$^4D_{1/2}, {}^2L_{15/2}, {}^2I_{13/2}, {}^4D_{7/2}, {}^2L_{17/2}$	3 500	208.66	1.783	1.943	0.0255

[a]In units of 10^{-20} cm^2. [b]Sample length 0.213 cm.

$CaY_2Mg_2Ge_3O_{12}$, and $La_2Ge_2O_5$, respectively. The JO fit to $Y_3Al_5O_{12}:Nd^{3+}$ has been previously reported[5] and since our measured absorption intensities for this crystal are essentially the same we refer the reader to Ref. 5. For $Gd_3Ga_5O_{12}:Nd^{3+}$ however, there are some discrepancies in the reported Ω_λ parameters.[9,10] Table V lists the Ω_λ parameters obtained by the present study and includes those for $Y_3Al_5O_{12}:Nd^{3+}$ for comparative purposes. Also listed are the parameters for $YVO_4:Nd^{3+}$. Finally the table contains two sets of parameters for $Gd_3Ga_5O_{12}:Nd^{3+}$ obtained by others. Our measurements confirm the results of Ref. 9.

From Table V it is seen that the Ω_2 intensity

TABLE IV. Absorbances, measured S_m, and calculated S_c line strengths for $La_2Be_2O_5:Nd^{3+}$[b] at 300 °K.

Excited state $\|4f^n[S',L'],J'\rangle$	$\bar{\lambda}$ (Å)	$\int\alpha(\lambda)\,d\lambda\left[\frac{\text{Å}}{\text{cm}}\right]$	S_m^a	S_c^a	$(\Delta S)^2$
$^4I_{13/2}$	24 000	...	...	...	...
$^4I_{15/2}$	16 000	55.10	0.169	0.273	0.0174
$^4F_{3/2}$	8 800	264.09	1.478	1.338	0.0197
$^4F_{5/2}, {}^2H2_{9/2}$	8 100	719.15	4.360	4.214	0.0214
$^4F_{7/2}, {}^4S_{3/2}$	7 500	611.30	3.990	4.186	0.0383
$^4F_{9/2}$	6 850	38.25	0.272	0.284	0.0002
$^2H2_{11/2}$	6 300	11.07	0.085	0.076	0.0001
$^4G_{5/2}, {}^2G1_{7/2}$	5 850	607.62	5.012	5.049	0.0013
$^4G_{7/2}, {}^4G_{9/2}, {}^2K_{13/2}$	5 250	264.78	2.411	1.874	0.2887
$^2G1_{9/2}, {}^2D_{3/2}, {}^2K_{15/2}, {}^4G_{11/2}$	4 750	58.42	0.582	0.429	0.0233
$^2D_{5/2}, {}^2P_{1/2}$	4 320	12.10	0.131	0.192	0.0037
$^4D_{3/2}, {}^4D_{5/2}, {}^2I_{11/2}, {}^4D_{1/2}, {}^2L_{15/2}, {}^2I_{13/2}, {}^4D_{7/2}, {}^2L_{17/2}$	3 480	200.44	2.576	2.865	0.0835

[a]In units of 10^{-20} cm^2. [b]Sample length 0.108 cm.

TABLE V. Intensity parameters for Nd^{3+} at 300 °K (units of 10^{-20} cm^2).

Host	Ω_2	Ω_4	Ω_6	Reference
$Y_3Al_5O_{12}$:Nd	0.2	2.7	5.0	5
$YAlO_3$:Nd	1.24	4.68	5.85	12
$CaY_2Mg_2Ge_3O_{12}$:Nd	0.93	2.94	4.41	this work
$La_2Be_2O_5$:Nd	2.11	4.39	6.04	this work
YVO_4:Nd	5.88	4.08	5.11	13
$Gd_3Ga_5O_{12}$:Nd	0.05	3.25	3.66	this work
$Gd_3Ga_5O_{12}$:Nd	0	3.3	3.7	9
$Gd_3Ga_5O_{12}$:Nd	0	3.7	3.7	10

parameter varies a great deal more from host to host than do the parameters Ω_4 and Ω_6. This variation of Ω_2 is due to so-called "hypersensitive transitions."[19] Most of the $f \rightarrow f$ transitions of the trivalent rare earths have intensities which are not greatly affected by the environment of the ion. A few, however, are very sensitive to environment and are therefore called hypersensitive transitions. It has been noted[20] that all known hypersensitive transitions obey the selection rules $|\Delta J| \leq 2$, $|\Delta L| \leq 2$, and $S = 0$ and that these are just the selection rules on the reduced matrix element $\langle || U^{(2)} || \rangle$. Hence it is concluded that hypersensitivity is a peculiar sensitivity of Ω_2 to the environment and therefore any transition with an intensity dominated by the value $\langle || U^{(2)} || \rangle$ is hypersensitive. Several theories both quantitative and qualitative have been put forward to explain this phenomena.[19] We will not discuss these here but rather simply note the significance of the Ω_2 parameter in laser design.

Only the transition $^4I_{9/2} \rightarrow {}^4G_{5/2}$ depends strongly on the matrix element $\langle || U^{(2)} || \rangle$. For this case $|\langle || U^{(2)} || \rangle| = 0.898$, while in all the other absorptions $|\langle || U^{(2)} || \rangle|$ is less than 0.075. Hence the $^4I_{9/2} \rightarrow {}^4G_{5/2}$ transition in Nd^{3+} is hypersensitive and furthermore the parameter Ω_2 will be determined almost entirely by the strength of this band. Inspection of Table V shows that YVO_4Nd^{3+} has the largest Ω_2 parameters and this is due to its relatively stronger $^4I_{9/2} \rightarrow {}^4G_{5/2}$ absorption band. The size of the Ω_2 parameter is important in determining the pumping efficiency of a Nd^{3+} laser crystal at the wavelength of the $^4I_{9/2} \rightarrow {}^4G_{5/2}$ transition, 5800 Å. Since the solar spectrum peaks near 5000 Å, YVO_4:Nd^{3+} would be more efficient in a solar-pumping scheme than the other hosts in Table V, particularly $Y_3Al_5O_{12}$:Nd^{3+} its main competitor. Thus YVO_4:Nd^{3+} would be a better solar-pumped laser candidate for space applications than $Y_3Al_5O_{12}$:Nd^{3+}. YVO_4:Nd^{3+} would also be more efficient than $Y_3Al_5O_{12}$ when pumped by a dye laser (Rhodamine 6G).

We now use the JO intensity parameters calculated from the absorption spectrum to compute fluorescence transition probabilities for these Nd^{3+}-doped crystals. The only excited J manifold that is not relaxed predominantly by multiphonon processes is the $^4F_{3/2}$ manifold. This manifold fluoresces in four bands centered at 0.88, 1.06, 1.35, and 1.8 μm corresponding to transitions from $^4F_{3/2} \rightarrow {}^4I_{9/2}$, $^4I_{11/2}$, $^4I_{13/2}$, and $^4I_{15/2}$, respectively. Using Eq. (6) the transition probabilities of these four bands can be evaluated and subsequent application of Eqs. (7) and (8) yield the radiative lifetime and branching ratios of the metastable $^4F_{3/2}$ level. Inspection of Eq. (5) shows that the Ω_λ parameters depend on the experimental absorption intensities through a constant which contains the ion concentration N. Hence the absolute values of the Ω_λ reflect the accuracy of the concentration. For dilute systems (where ions are doped as impurities in a lattice at very low concentration) the ion concentration is very difficult to measure accurately. Most workers claim an accuracy of ±15%, however, this estimate may be questionable.[17,21] The principal techniques used in the determination of N are x-ray fluorescence, electron microprobe, emission spectroscopy, and wet chemical analysis. In this study the values used for the Nd^{3+} ion concentration in $Gd_3Ga_5O_{12}$, $CaY_2Mg_2Ge_3O_{12}$, and $La_2Be_2O_5$ were obtained by equating the radiative lifetime of Eq. (12) to the measured concentration-independent fluorescence lifetime. Before explaining this procedure we define the pertinent quantities.

The total transition rate A_T from an excited manifold J to a lower manifold J' is given by

$$A_T(J,J') = A_R(J,J') + A_{NR}(J,J') \quad , \tag{19}$$

where A_R and A_{NR} refer to the radiative and nonradiative rates from J to J', respectively. This is equivalent to writing

$$\frac{1}{\tau} = \frac{1}{\tau_R} + \frac{1}{\tau_{NR}} \quad , \tag{20}$$

where τ is the observed fluorescence lifetime of level J with τ_R and τ_{NR} are the radiative and nonradiative lifetimes, respectively. The radiative quantum efficiency (henceforth referred to as the quantum efficiency) is given by

$$\eta = \frac{A_R}{A_R + A_{NR}} = \frac{\tau}{\tau_R} \quad . \tag{21}$$

Our basic assumption in estimating the Nd^{3+} concentration N of the samples is that the $^4F_{3/2}$ level decays entirely by a radiative pathway implying that $A_{NR} = 0$ and $\eta = 1$. This enables us to establish an upper limit on the absolute values of the Ω_λ parameters. (Clearly the quantum efficiency cannot exceed unity.) This approach was taken because of the prohibitive cost and sometimes unreliable results of

TABLE VI. Fluorescence properties of $Gd_3Ga_5O_{12}$:Nd^{3+} at 300 °K. Total radiative rate = 4000 sec^{-1}.

Transition	$A(J,J')$[a] Transition rate (sec^{-1})	τ(μsec)	Branching ratio
$^4F_{3/2} \rightarrow {}^4I_{9/2}$	1740	575	0.435
$^4F_{3/2} \rightarrow {}^4I_{11/2}$	1821	549	0.455
$^4F_{3/2} \rightarrow {}^4I_{13/2}$	428	2 336	0.107
$^4F_{3/2} \rightarrow {}^4I_{15/2}$	11	90 910	0.003

[a]Based on $N = 5.45 \times 10^{19}/cm^3$ and $\eta = 1.0$.

determining N by the methods previously mentioned. With an upper limit of the Ω_λ parameters established the next step would be to measure the nonradiative transition rate from level J' and thereby obtain the correct quantum efficiency and the correct radiative transition rate.

The nonradiative transition rate from an excited level can be due to: (a) multiphonon emission which is due to interactions of ions with crystal lattice vibrations; (b) ion-ion interactions which become dominant at higher concentrations. At a low enough concentration the ions become sufficiently separate that ion-ion interactions are negligible and the only nonradiative relaxation mechanism is multiphonon emission. Below this concentration the fluorescence lifetime remains constant and hence is concentration independent. This is the meaning of the concentration-independent fluorescence lifetime referred to previously.

The intensity parameters listed in Table V and the line strengths listed in Tables II–IV were obtained from ion concentrations extrapolated from the concentration-independent fluorescence lifetime assuming a quantum efficiency of unity. The concentration-independent fluorescence lifetimes for Nd^{3+} in $Gd_3Ga_5O_{12}$, $CaY_2Mg_2Ge_3O_{12}$, and $La_2Be_2O_5$ are 250,[9] 298,[22] and 150 μsec,[18] respectively, leading to ion concentrations of $5.45 \times 10^{19}/cm^3$, $1.84 \times 10^{20}/cm^3$, and $1.06 \times 10^{20}/cm^3$, respectively.

In order to use Eqs. (6), (7), and (8) the $^4F_{3/2} \rightarrow {}^4I_{9/2}$, $^4I_{11/2}$, $^4I_{13/2}$, $^4I_{15/2}$ transition matrix elements, mean transition wavelengths $\bar{\lambda}$, and refractive indices $n(\bar{\lambda})$ are needed. The matrix elements were taken from Krupke[5] and the values for $\bar{\lambda}$ were taken from Koningstein[23] for Nd^{3+} in $Y_3Al_5O_{12}$ since the positions of the centers of gravity of the ^4I_J and $^4F_{3/2}$ manifolds do not vary much from crystal to crystal.[24] The refractive indices were taken from the previously given Sellmeier equations.

Using the Ω_λ of Table V the fluorescence transition probabilities and branching ratios for Nd^{3+} in $Gd_3Ga_5O_{12}$, $CaY_2Mg_2Ge_3O_{12}$, and $La_2Be_2O_5$ were calculated. The results are listed in Tables VI, VII, and VIII, respectively. We include in Table IX the fluorescence properties of $Y_3Al_5O_{12}$:Nd^{3+} taken from Ref. 5 for comparison.

A lower limit for the Ω_λ of Nd^{3+} in $CaY_2Mg_2Ge_3O_{12}$ and $La_2Be_2O_5$ was established by assuming a maximum ion concentration in each crystal based on the percentage of Nd^{3+} placed in the melt when the crystal was grown. These data were not available for the $Gd_3Ga_5O_{12}$ sample used. For $La_2Be_2O_5$ the percent atomic concentration of Nd^{3+} placed on the melt when the crystal was grown was

TABLE VII. Fluorescence properties of $CaY_2Mg_2Ge_3O_{12}$:Nd^{3+} at 300 °K. Total radiative rate = 3355 sec^{-1}.

Transition	$A(J,J')$[a] Transition rate (sec^{-1})	τ(μsec)	Branching ratio
$^4F_{3/2} \rightarrow {}^4I_{9/2}$	1318	759	0.393
$^4F_{3/2} \rightarrow {}^4I_{11/2}$	1620	617	0.483
$^4F_{3/2} \rightarrow {}^4I_{13/2}$	407	2 457	0.121
$^4F_{3/2} \rightarrow {}^4I_{15/2}$	10.4	96 154	0.003

[a]Based on $N = 1.84 \times 10^{20}/cm^3$ and $\eta = 1.0$.

TABLE VIII. Fluorescence properties of $La_2Be_2O_5:Nd^{3+}$ at 300 °K. Total radiative rate = 6671/sec.

Transition	$A(J,J')$[a] Transition rate (sec^{-1})	τ(μsec)	Branching ratio
$^4F_{3/2} \rightarrow {}^4I_{9/2}$	2716	368	0.407
$^4F_{3/2} \rightarrow {}^4I_{11/2}$	3160	317	0.474
$^4F_{3/2} \rightarrow {}^4I_{13/2}$	776	1 289	0.116
$^4F_{3/2} \rightarrow {}^4I_{15/2}$	18.8	53 192	0.003

[a]Based on $N = 1.06 \times 10^{20}/cm^3$ and $\eta = 1.0$.

1.2 at.%. The ion concentration is calculated as follows. The lattice parameters for $La_2Be_2O_5$ are[25] $a_0 = 7.536$ Å, $b_0 = 7.348$ Å, and $c_0 = 7.439$ Å with the unit cell being monoclinic with a volume of $V = a_0 b_0 c_0 = 4.12 \times 10^{-22}\ cm^3$. There are four chemical formulas of $La_2Be_2O_5$ in each unit cell and the Nd^{3+} ions substitute for the La atoms which are of comparable size. Therefore if every La atom is replaced by an Nd^{3+} ion the concentration would be

$$\frac{Nd^{3+}}{cm^3} = \frac{8}{(4.12 \times 10^{-22}\ cm^3)} = 1.942 \times \frac{10^{22}}{cm^3} .$$

In our case only 1.2% or 0.012 of the atoms are replaced yielding an ion concentration of $2.33 \times 10^{20}/cm^3$. Using this concentration the lower limit of the Ω_λ parameters for $La_2Be_2O_5:Nd^{3+}$ are found to be $\Omega_2 = 0.95 \times 10^{-20}\ cm^2$, $\Omega_4 = 1.99 \times 10^{-20}\ cm^2$, and $\Omega_6 = 2.73 \times 10^{-20}\ cm^2$ with the lower limit of the quantum efficiency being $\eta = 0.453$.

Similarly for $CaY_2Mg_2Ge_3O_{12}:Nd^{3+}$ we know that the percent atomic concentration added to the melt was 6%. $CaY_2Mg_2Ge_3O_{12}$ has a cubic garnet structure like $Y_3Al_5O_{12}$ and this becomes clear when its chemical formula is rewritten $CaY_2Mg_2(GeO_4)_3$. The structure of the unit cell is body centered with lattice parameters $a_0 = b_0 = c_0 = 12.29 \pm 0.03$ Å as determined by x-ray diffraction analysis.[26] The volume of the unit cell is therefore $V = a_0 b_0 c_0 = 1.856 \times 10^{-21}\ cm^3$, with eight chemical formulas of $CaY_2Mg_2(GeO_4)_3$ in each shell. The Nd^{3+} ions in this case substitute for the yttrium atoms and therefore the 6 at.% concentration is given by

$$\frac{Nd^{3+}}{cm^3} = \frac{(16 \times 0.06)}{(1.856 \times 10^{-21}/cm^3)} = 5.17 \times \frac{10^{20}}{cm^3} .$$

Using this concentration we get lower limit values for the $CaY_2Mg_2Ge_3O_{12}:Nd^{3+}$ intensity parameters of $\Omega_2 = 0.33 \times 10^{-20}\ cm^2$, $\Omega_4 = 1.04 \times 10^{-20}\ cm^2$, and $\Omega_6 = 1.55 \times 10^{-20}\ cm^2$ with a lower limit on the quantum efficiency of $\eta = 0.356$.

The major pump bands for Nd^{3+} in $Y_3Al_5O_{12}$, $CaY_2Mg_2Ge_3O_{12}$, and $La_2Be_2O_5$ were normalized to their respective ion concentrations (those extrapolated from the fluorescence lifetimes assuming $\eta = 1$) and compared in Figs. 2 and 3. These pump bands were centered in the yellow at 5800 Å corresponding to the $^4I_{9/2} \rightarrow {}^4G_{5/2}, {}^2G1_{7/2}$ transition (Fig. 2) and in the near infrared at 7500 and 7900 Å corresponding to the $^4I_{9/2} \rightarrow {}^4F_{7/2}, {}^4S_{3/2}$ and $^4I_{9/2} \rightarrow {}^4F_{5/2}, {}^2H2_{9/2}$ (Fig. 3) transitions, respectively. It is seen that the absorption lines of $La_2Be_2O_5:Nd^{3+}$ are broader and stronger than those of $Y_3Al_5O_{12}:Nd^{3+}$ and $CaY_2Mg_2Ge_3O_{12}:Nd^{3+}$. Hence in a broadband pumping configuration (xenon or krypton flashlamp) $La_2Be_2O_5:Nd^{3+}$ will have a larger absorption cross section than $Y_3Al_5O_{12}:Nd^{3+}$ or $CaY_2Mg_2Ge_3O_{12}:Nd^{3+}$ and

TABLE IX. Fluorescence properties of $Y_3Al_5O_{12}:Nd^{3+}$ at 300 °K. Total radiative rate = 3868/sec.

Transition	$A(J,J')$[a] Transition rate (sec^{-1})	τ(μsec)	Branching ratio
$^4F_{3/2} \rightarrow {}^4I_{9/2}$	1420	703	0.37
$^4F_{3/2} \rightarrow {}^4I_{11/2}$	1940	518	0.50
$^4F_{3/2} \rightarrow {}^4I_{13/2}$	493	2 000	0.13
$^4F_{3/2} \rightarrow {}^4I_{15/2}$	15	112 000	0.003

[a]Based on $N = 1.06 \times 10^{20}/cm^3$ and $\eta = 0.91$.

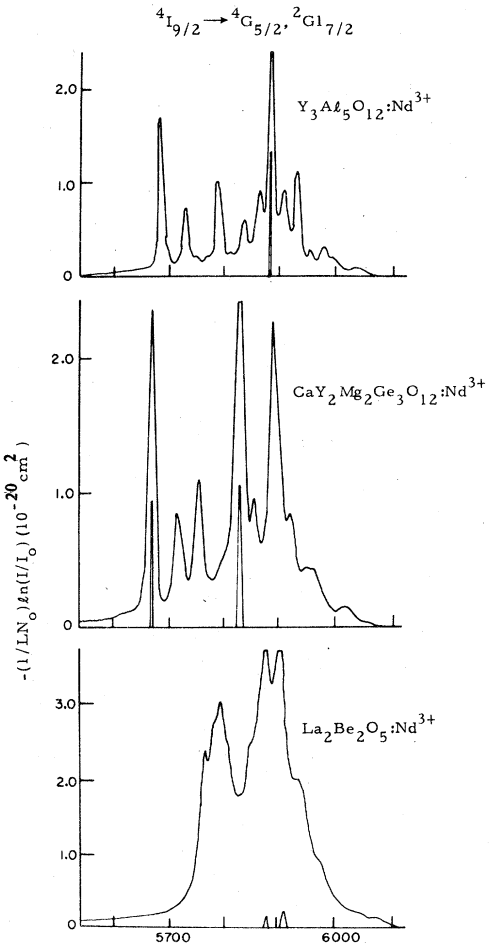

FIG. 2. Comparison of the 5800-Å absorption band of Nd^{3+} in $Y_3Al_5O_{12}$, $CaY_2Mg_2Ge_3O_{12}$, and $La_2Be_2O_5$. L is the sample length and N_0 is the Nd^{3+} concentration.

hence be more efficient as a laser material. If a pump source of a specific wavelength is used the sharp structure of the garnet hosts ($Y_3Al_5O_{12}$ and $CaY_2Mg_2Ge_3O_{12}$) may deem them less efficient due to a mismatch of the pump wavelength and an absorption peak.

Absorption from the metastable $^4F_{3/2}$ level to higher-lying configurations is a mechanism which tends to degrade Nd^{3+} laser performance because it reduces the population inversion of the upper laser level. A pulsed Q-switched $Y_3Al_5O_{12}:Nd^{3+}$ laser will have an excited population density of about $10^{18}/cm^3$ just prior to switching, and a cw $Y_3Al_5O_{12}:Nd^{3+}$ laser will have an excited population of $5 \times 10^{16}/cm^3$ at steady state. In order to evaluate the effect of excited-state absorption we must know the absorption strengths of transitions originating on the $^4F_{3/2}$ level which match the wavelength of radiation likely to be in the laser cavity. These would include the

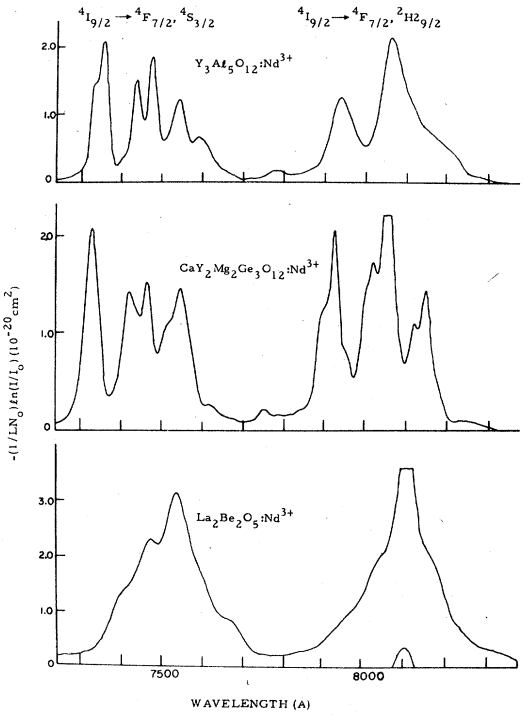

FIG. 3. Comparison of the near-infrared absorption band of Nd^{3+} in $Y_3Al_5O_{12}$, $CaY_2Mg_2Ge_3O_{12}$, and $La_2Be_2O_5$. L is the sample length and N_0 is the Nd^{3+} concentration.

wavelengths 0.88, 1.06, and 1.35 μm the approximate wavelengths at which there are strong krypton pump lamp lines and 0.5321 μm which is the doubled radiation of 1.06-μm $Y_3Al_5O_{12}:Nd^{3+}$. In Table X which is taken from Ref. 5 are listed the transitions and corresponding matrix elements which are closest in wavelength to the wavelengths listed in the above paragraph. For Table X it can be seen that the line strengths of the excited-state transitions $^4F_{3/2} \rightarrow {}^2P_{1/2}$ and $^4F_{2/3} \rightarrow {}^2D1_{5/2}$ are very small. Hence excited-state absorption will not be an appreciable loss mechanism for an Nd^{3+} laser operated at 0.88 μm or

TABLE X. Transition-matrix elements for excited $^4F_{3/2}$ absorption transitions in Nd^{3+}.

$\lvert 4f^n[S',L'],J'\rangle$	$\bar{\lambda}$ (μm)	$\lvert\langle U^{(2)}\rangle\rvert^2$	$\lvert\langle U^{(4)}\rangle\rvert^2$	$\lvert\langle U^{(6)}\rangle\rvert^2$
$^4G_{7/2}$	1.35	0.127	0.062	0
$^2G1_{9/2}$	1.06	0	0.022	0.425
$^2P_{1/2}$	0.88	0.015	0	0
$^2D1_{5/2}$	0.80	0	0.0015	0
$^4D_{7/2}$	0.5321	0.0017	0.100	0

pumped by a krypton lamp. The excited-state absorption $^4F_{3/2} \rightarrow {}^4G1_{9/2}$ has a total line strength comparable to the line strength of the 1.06-μm laser band.[5] This is consistent with experimental observations made by Vance[27] for Nd^{3+} in soda lime glass. Since the $^4F_{3/2} \rightarrow {}^4G1_{9/2}$ transition depends primarily on the matrix element $|\langle U^{(6)} \rangle|^2$ the size of the Ω_6 parameter will determine its line strength. Since Ω_6 does not vary much from host to host for Nd^{3+} (compared to Ω_2) the strength of this excited-state transition should be about the same in all hosts. For a glass host the absorption manifolds are inhomogeneously broadened and the chance of an energy match between the 1.06-μm fluorescence and excited-state transition is rather high. For sharp Stark splitting of the absorption lines as in $Y_3Al_5O_{12}$:Nd^{3+}, $Gd_3Ga_5O_{12}$:Nd^{3+}, and $CaY_2Mg_2Ge_3O_{12}$:Nd^{3+} the match is less probable and a low-temperature absorption spectrum of the $^4I_{9/2} \rightarrow {}^2G1_{7/2}$ manifold would be required to determine if any of its Stark components matched the wavelength of the laser line. Nd^{3+} in $La_2Be_2O_5$ has slightly broader absorption lines than in $Gd_3Ga_5O_{12}$, $CaY_2Mg_2Ge_3O_{12}$, or $Y_3Al_5O_{12}$ and hence would exhibit a greater loss due to excited-state absorption than these three crystals. The line strength of the $^4F_{3/2} \rightarrow {}^4G_{7/2}$ transition is dependent primarily on the matrix element $|\langle U^{(2)} \rangle|^2$ and hence on the intensity parameter Ω_2. Ω_2 is the only parameter which is particularly sensitive to the ion environment. Hence larger variations in the excited-state absorption line strength at 1.35 μm can be expected than at the other wavelengths (1.06, 0.88, 0.8, 0.5321 μm) for different hosts. This line strength will be larger for systems such as Y_2O_3:Nd^{3+} and YVO_4:Nd^{3+} where the Ω_2 parameters are relatively large (8.6×10^{-20} cm^2 and 5.88×10^{-20} cm^2, respectively) compared to the garnets ($Y_3Al_5O_{12}$, $Gd_3Ga_5O_{12}$, and $CaY_2Mg_2Ge_3O_{12}$) where the Ω_2 are nearly zero. Hence these systems (YVO_4 and Y_2O_3) will operate with greater excited-state absorption loss at 1.35 μm than the garnet systems.

B. Validity of JO theory in Nd^{3+} fluorescence transitions

We now proceed to apply the JO theory in the analysis of the fluorescence of Nd^{3+} laser transitions. Specifically we show from the JO theory that the ratio of 1.06 to 1.35 μm fluorescence band intensities varies linearly with the ratio Ω_4/Ω_6 for a series of Nd^{3+}-doped crystals. Experimental verification of this linearity shows the validity of the JO theory in describing these fluorescence transitions.

The strength of the fluorescence bands of Nd^{3+} are given by the equation

$$A(J,J') = \frac{K}{\bar{\lambda}^3} S(J,J') \ , \tag{22}$$

with

$$K \equiv \tfrac{1}{9}[32\pi^3 \alpha_f / 3(2J+1)] n (n^2+2)^2 \ .$$

Since the refractive index n of the host materials investigated did not vary appreciably with $\bar{\lambda}$ over the wavelength region of the Nd^{3+} fluorescence (0.9 to 1.8 μm) the factor K in Eq. (22) is assumed to be wavelength independent. Substitution of Eq. (22) into Eq. (8) leads to an expression for the fluorescence branching ratios given by

$$\beta(J,J') = \frac{\frac{1}{\bar{\lambda}^3_{J,J'}} \sum\limits_{\lambda=2,4,6} \Omega_\lambda |\langle J \| U^{(\lambda)} \| J' \rangle|^2}{\sum\limits_{J,J'} \frac{1}{\bar{\lambda}^3_{J,J'}} \sum\limits_{\lambda=2,4,6} \Omega_\lambda |\langle J \| U^{(\lambda)} \| J' \rangle|^2} \ , \tag{23}$$

where the matrix elements of Eq. (23) are given by

$$\langle J \| U^{(\lambda)} \| J' \rangle = \sum_{\substack{S,S' \\ L,L'}} \delta_{SS'} (-1)^{J+L'+S+\lambda} C(SLJ) C(S'L'J') [(2J+1)(2J'+1)]^{1/2} \begin{Bmatrix} J & J' & \lambda \\ L' & L & S \end{Bmatrix} \langle SL \| U^{(\lambda)} \| S'L' \rangle \ .$$

Inspection of this equation makes it clear that the matrix elements obey selection rules on J and J' due to triangle relations[28] that are imposed on the $6j$ symbol

$$\begin{Bmatrix} J & J' & \lambda \\ L' & L & S \end{Bmatrix} .$$

Using the triangle relations we find in Nd^{3+} that for the $^4F_{3/2} \rightarrow {}^4I_{9/2}$ (0.9 μm) and $^4F_{3/2} \rightarrow {}^4I_{11/2}$ (1.06 μm) transitions we have $\langle \| U^{(2)} \| \rangle = 0$ and for the $^4F_{3/2} \rightarrow {}^4I_{13/2}$ (1.35 μm) and $^4F_{3/2} \rightarrow {}^4I_{15/2}$ (1.8 μm) transitions we have $\langle \| U^{(2)} \| \rangle = \langle \| U^{(4)} \| \rangle = 0$.

We find therefore that the ratio of $\beta(\frac{3}{2}, \frac{11}{2})$ to $\beta(\frac{3}{2}, \frac{13}{2})$ is linear in X and is

$$R = \frac{\beta(\frac{3}{2},\frac{11}{2})}{\beta(\frac{3}{2},\frac{13}{2})} = \left[\frac{|\langle \frac{3}{2} \| U^{(4)} \| \frac{11}{2} \rangle|^2}{|\langle \frac{3}{2} \| U^{(6)} \| \frac{13}{2} \rangle|^2} \left(\frac{\bar{\lambda}_{1.35\ \mu m}}{\bar{\lambda}_{1.06\ \mu m}} \right)^3 \right] + \frac{|\langle \frac{3}{2} \| U^{(6)} \| \frac{11}{2} \rangle|^2}{|\langle \frac{3}{2} \| U^{(6)} \| \frac{13}{2} \rangle|^2} \left(\frac{\bar{\lambda}_{1.35\ \mu m}}{\bar{\lambda}_{1.06 \mu m}} \right)^3 . \tag{25}$$

The validity of the three-parameter JO theory applied to fluorescence transitions in Nd^{3+} could be verified by showing the linearity between R and X

predicted by Eq. (25). Since the X parameter contains parameters from the crystal-field potential of a crystal host we expect to see variations in X and hence R with host material. Thus the procedure to follow is to measure R and X for a series of Nd^{3+}-doped materials.

The parameter X is available for a larger number of Nd^{3+}-doped crystals including $CaY_2Mg_2Ge_3O_{12}$, $La_2Be_2O_5$, and YVO_4 which are listed in Table V of this paper. The parameter R is the ratio of the 1.06- to 1.35-μm fluorescence band intensities and has been previously measured by the authors[29] for Nd^{3+} in 25 crystal and glass hosts. The experimental technique used in this prior work has been reiterated in Sec. II B of this paper.

Table XI contains 14 Nd^{3+}-doped crystals which have available R parameters and have also been JO analyzed to obtain the intensity parameters Ω_2, Ω_4, and Ω_6. In the prior work[29] we have measured all the R values of the crystals shown in Table XI except for the cubic mixed-crystal systems BaF_2-LuF_3, BaF_2-CeF_3, $Lu_3Sc_2Al_3O_{12}$, and ZrO_2-Y_2O_3 for which the R parameters are taken from Ref. 30.

Equation (25) predicts a linear relation $R = AX + B$ where A and B are the ratios of matrix elements and mean transition wavelengths. These matrix elements depend entirely on the intermediate-coupled wave functions. We proceed to test how well the R vs X data fitted the linear relation $R = AX + B$. The constants A and B were varied by using different wave functions in the calculation of the matrix elements. The matrix elements $\langle \| U^{(4)} \| \rangle$ and $\langle \| U^{(6)} \| \rangle$ were calculated by using three different wave functions. The intermediate-coupled wave functions determined by Rajnak[31] were used for one determination.[32] Another calculation of these matrix elements was done by Krupke[5] using a truncated version of the intermediate-coupled wave functions. Since the initial and final states producing the fluorescence were nearly pure LS, only the largest component of the intermediate-coupled wave function was retained. This truncation is not possible for absorption matrix elements since many of the upper absorption states are rather mixed. Matrix elements based on pure LS wave functions were computed for comparison. The matrix elements obtained by these different wave functions are listed in Table II of Ref. 29. The results of the truncated wave functions fitted the data well, but the results obtained by using the full intermediate-coupled wave functions failed to give meaningful results. This is shown by the fact that when the full intermediate-coupled wave functions are used, Eq. (25) becomes $R = 1.363\,X + 3.896$, which yields negative X parameter for 9 of 25 crystals. This seems to be an impossible situation.[33] We list for comparison three verisons of Eq. (25) obtained by using the different wave functions. They are: pure LS

$$R = 1.178X + 3.229 \ ,$$

truncated intermediate coupled

$$R = 1.167X + 3.185 \ , \qquad (26)$$

and intermediate coupled

$$R = 1.363X + 3.896 \ .$$

The values of $\bar{\lambda}$ used in the computation of these

TABLE XI. Fluorescence and absorption intensity parameters for Nd^{3+}-doped materials at 300 °K.

Sample	R	$X = \Omega_4/\Omega_6$	Ω_2^a	Ω_4^a	Ω_6^a	Reference
$YLiF_4$:Nd	3.66	0.54	1.9	2.7	5.0	10
BaF_2-LuF_3:Nd[b]	3.69	0.54	0.67	2.46	4.58	30
$CaY_2Mg_2Ge_3O_{12}$:Nd	3.76	0.67	0.93	2.94	4.41	this work
$Y_3Al_5O_{12}$:Nd	3.83	0.54	0.2	2.7	5.0	5
BaF_2-CeF_3:Nd[b]	3.83	0.51	0.43	2.30	4.50	30
$Lu_3Sc_2Al_3O_{12}$:Nd[b]	4.00	0.58	0.22	3.07	5.27	30
$YAlO_3$:Nd	4.00	0.80	1.24	4.68	5.85	12
ED2glass:Nd[c]	4.06	0.85	3.3	4.7	5.5	10
YVO_4:Nd	4.15	0.80	5.88	4.08	5.11	13
$La_2Be_2O_5$:Nd	4.20	0.73	2.11	4.39	6.04	this work
ZrO_2-Y_2O_3:Nd[b]	4.25	0.88	0.23	1.20	1.36	30
$Gd_3Ga_5O_{12}$:Nd(1)	4.46	0.89	0.05	3.25	3.66	this work
$Gd_3Ga_5O_{12}$:Nd(2)	4.46	1.00	0	3.7	3.7	10
LaF_3:Nd	4.61	1.03	0.35	2.57	2.50	35

[a] In units of 10^{-20} cm^2.

[b] R parameters taken from Ref. 30.

[c] Composition of ED2 glass in percentage by weight: $SiO_2 = 66.10\%$; $Al_2O_3 = 4.64\%$; $Li_2O = 16.00\%$; $CaO = 10.36\%$; $Nd_2O_3 = 3.13\%$; $CeO_2 = 0.45\%$; and $Fe_2O_3 = 4$ ppm.

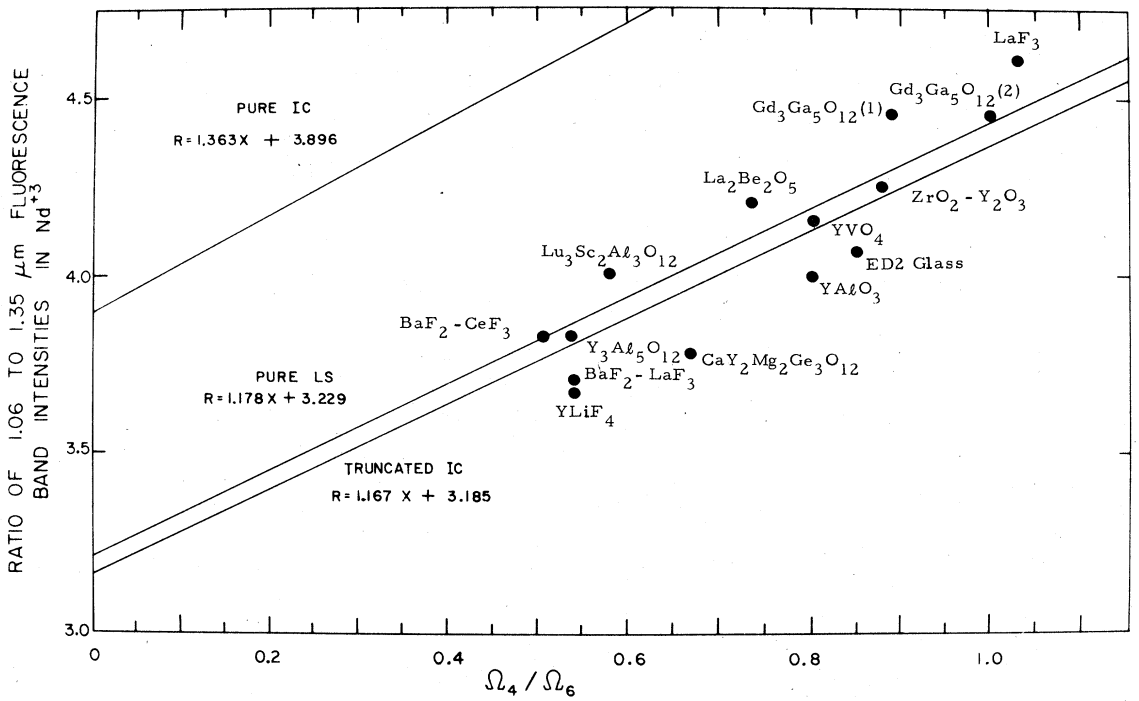

FIG. 4. R vs $X = \Omega_4/\Omega_6$ for a series of Nd^{3+}-doped crystals. The ratio of the fluorescence band intensities were directly measured while the ratio Ω_4/Ω_6 was obtained by a fit of the absorption data to the JO theory. The composition of ED2 glass is given in the footnote of Table XI.

equations were taken from Koningstein.[23]

The plots of Eqs. (26) along with the R vs X data of the 14 crystals in Table XI are shown in Fig. 4. It is clear that the linear equation based on the intermediate-coupled wave functions does not fit the data at all. The data generally follow the linear trend of the equations based on LS wave functions. This shows that the JO Eq. (25) is indeed applicable in describing the fluorescence and absorption transitions of Nd^{3+} in solids provided proper wave functions are used. A possible explanation of the failure of the intermediate-coupled wave functions to fit the R vs X data is in the way in which these wave functions are obtained, which is by empirical fittings to experimental energy levels. These calculations may reproduce the positions of the energy levels quite satisfactorily but it does not necessarily follow that the wave functions derived from these calculations are equally satisfactory. Even in the absence of other complications we see that the energies are essentially determined by the expectation values of r^{-1} and, therefore, the values of the wave functions for small r are most important. For dipole transition probabilities, the matrix components of r are of importance, and because of the factor r^2 difference as compared to the energies, the values of the wave functions at much larger values of r carry the heaviest weight.[34] For this reason the wave functions giving the best values of the energies may not necessarily give the best transition probabilities.

A problem of self-consistency arises when the wave functions for the fluorescence transition are changed in order to modify the constants A and B in the equation $R = AX + B$. The X parameter is obtained by fitting absorption strengths using intermediate-coupled wave functions. Changing these wave functions to LS wave functions would lead to nonsense in the fitting procedure since the upper absorption states are rather mixed. It should be noted, however, that in determining the parameter X the absorption data is fit with wave functions connecting the ground state $^4I_{9/2}$ and upper states whereas the evaluation of the fluorescence matrix elements in Eq. (25) contain wave functions originating on the $^4F_{3/2}$ level and terminating on the levels $^4I_{11/2}$ and $^4I_{13/2}$ and not the level $^4I_{9/2}$. Therefore the same sets of matrix elements are not used in the fluorescence and absorption intensity calculations.

*Present address: Optical Systems Department, The Aerospace Corporation, El Segundo, Calif. 90245.
†Present address: Hughes Research Laboratories, Malibu, Calif. 90265.

[1]O. Laporte, Z. Phys. 33, 135 (1924).
[2]J. H. Van Vleck, J. Chem. Phys. 41, 67 (1937).
[3]B. R. Judd, Phys. Rev. 127, 750 (1962).
[4]G. S. Ofelt, J. Chem. Phys. 37, 511 (1962).
[5]W. F. Krupke, IEEE J. Quantum Electron. QE-7, 153 (1971).
[6]W. F. Krupke, IEEE J. Quantum Electron. QE-8, 725 (1972).
[7]J. A. Caird and L. G. DeShazer, IEEE J. Quantum Electron. QE-11, 97 (1975).
[8]W. F. Krupke, IEEE J. Quantum Electron. QE-10, 450 (1974).
[9]W. F. Krupke, Opt. Commun. 12, 210 (1974).
[10]W. F. Krupke, IEEE Region VI Conference, Albuquerque, N.M., 1974 (unpublished).
[11]R. R. Jacobs and M. J. Weber, IEEE J. Quantum Electron. QE-12, 102 (1976).
[12]M. J. Weber and T. E. Varitimos, J. Appl. Phys. 42, 2996 (1971).
[13]T. S. Lomheim and L. G. DeShazer, J. Appl. Phys. 49, 5517 (1978).
[14]I. I. Sobel'mann, *An Introduction to the Theory of Atomic Spectra* (Perg mon, Oxford, 1972), p. 180.
[15]H. M. Crosswhite (private communication).
[16]W. B. Fowler and D. L. Dexter, Phys. Rev. 128, 2154 (1962)
[17]H. L. Wang, Ph.D. dissertation (University of Southern California, 1975).
[18]H. P. Jenssen, R. F. Begley, R. Webb, and R. C. Morris, J. Appl. Phys. 47, 1496 (1976).
[19]R. D. Peacock, *Structure and Bonding* (Springer, New York, 1975), Vol. 22, p. 83.
[20]C. K. Jorgensen and B. R. Judd, Mol. Phys. 8, 281 (1964).
[21]J. K. Guha, Ph.D. dissertation (University of Southern California, 1973).
[22]M. Birnbaum, A. W. Tucker, and C. L. Fincher, J. Appl. Phys. 49, 2984 (1978).
[23]J. A. Koningstein, J. Chem. Phys. 44, 3957 (1966).
[24]A. A. Kaminskii and L. Li, Phys. Status Solidi A 26, 593 (1974).
[25]L. A. Harris and H. L. Yakel, Acta Crystallogr. B 24, 672 (1968).
[26]Dr. N. Parobek, Hi-Rel Labs, Monrovia, Calif. (private communication).
[27]M. E. Vance, IEEE J. Quantum Electron. QE-6, 249 (1970).
[28]M. Rotenburg, R. Bivens, N. Metropolis, and J. K. Wooten, *The 3-j and 6-j Symbols* (Technology, Cambridge, Mass., 1959).
[29]T. S. Lomheim and L. G. DeShazer, Opt. Commun. 24, 89 (1978).
[30]A. A. Kaminskii and L. Li, Phys. Status Solidi A 26, K21 (1974).
[31]K. Rajnak, J. Chem. Phys. 43, 847 (1965).
[32]J. Caird, Ph.D. dissertation (University of Southern California, 1975).
[33]Negative values of X are excluded by the positiveness of the transition intensity. For Nd^{3+}, the transition $^4I_{9/2} \rightarrow {}^2P_{1/2}$ is due entirely to the Ω_4 term so Ω_4 must be positive. Likewise the Ω_6 parameter must be positive since $^4F_{3/2} \rightarrow {}^4I_{13/2}$ is due to an Ω_6 term alone.
[34]G. H. Dieke, in *Spectra and Energy Levels of Rare Earth Ions in Crystals,* edited by H. M. Crosswhite and H. Crosswhite (Interscience, New York, 1968), p. 65.